Spectral relationships for atmospheric correction. I. Validation of red and near infra-red marine reflectance relationships

C. Goyens,[1] C. Jamet,[1*] and K. G. Ruddick[2]

[1] *CNRS, UMR 8187, Université Lille Nord de France, ULCO, LOG, F-62930 Wimereux, France*
[2] *Management Unit of the North Sea Mathematical Models (MUMM), Royal Belgian Institute for Natural Sciences (RBINS), 100 Gulledelle, B-1200 Brussels, Belgium*

[*] *cedric.jamet@univ-littoral.fr*

Abstract: The present study provides an extensive overview of red and near infra-red (NIR) spectral relationships found in the literature and used to constrain red or NIR-modeling schemes in current atmospheric correction (AC) algorithms with the aim to improve water-leaving reflectance retrievals, $\rho_w(\lambda)$, in turbid waters. However, most of these spectral relationships have been developed with restricted datasets and, subsequently, may not be globally valid, explaining the need of an accurate validation exercise. Spectral relationships are validated here with turbid *in situ* data for $\rho_w(\lambda)$. Functions estimating $\rho_w(\lambda)$ in the red were only valid for moderately turbid waters ($\rho_w(\lambda_{NIR}) < 3.10^{-3}$). In contrast, bounding equations used to limit $\rho_w(667)$ retrievals according to the water signal at 555 nm, appeared to be valid for all turbidity ranges presented in the *in situ* dataset. In the NIR region of the spectrum, the constant NIR reflectance ratio suggested by Ruddick et al. (2006) (Limnol. Oceanogr. **51**, 1167-1179), was valid for moderately to very turbid waters ($\rho_w(\lambda_{NIR}) < 10^{-2}$) while the polynomial function, initially developed by Wang et al. (2012) (Opt. Express **20**, 741-753) with remote sensing reflectances over the Western Pacific, was also valid for extremely turbid waters ($\rho_w(\lambda_{NIR}) > 10^{-2}$). The results of this study suggest to use the red bounding equations and the polynomial NIR function to constrain red or NIR-modeling schemes in AC processes with the aim to improve $\rho_w(\lambda)$ retrievals where current AC algorithms fail.

© 2013 Optical Society of America

OCIS codes: (010.0010) Atmospheric and oceanic optics; (010.1285) Atmospheric correction; (010.4450) Oceanic optics; (010.1690) Color.

References and links

1. H. R. Gordon and M. Wang, "Retrieval of water-leaving radiance and aerosol optical thickness over the oceans with SeaWiFS: A preminilary algorithm," Appl. Opt. **33**, 443–452 (1994).
2. H. R. Gordon, "Removal of atmospheric effects from satellite imagery of the oceans," Appl. Opt. **17**, 1631–1636 (1978).
3. D. A. Siegel, M. Wang, S. Maritorena, and, W. Robinson, "Atmospheric correction of satellite ocean color imagery: The black pixel assumption," Appl. Opt. **39**(21), 3582–3591 (2000).

4. R. P. Stumpf, R. A. Arnone, J. R. W. Gould, P. M. Martinolich, and, V. Ransibrahmanakul, "A partially coupled ocean-atmosphere model for retrieval of water-leaving radiance from SeaWiFS in coastal waters," in *SeaW-iFS Postlaunch Technical Report Series, Volume 22, NASA Tech. Memo. 2003-206892*, S. B. Hooker and E. R. Firestone, eds., (NASA Goddard Space Flight Center, Greenbelt, Maryland), pp. 51–59 (2003).

5. S. W. Bailey, B. A. Franz, and, P. J. Werdell, " Estimations of near-infrared water-leaving reflectance for satellite ocean color data processing," Opt. Express **18**(7), 7521–7527 (2010).

6. C. Jamet, S. Thiria, C. Moulin, and, M. Crepon " Use of neuro-variational inversion for retrieving oceanic and atmospheric constituents from ocean color imagery, " J. Atmos. Ocean. Tech. **22**(4), 460–464 (2005).

7. T. Schroeder, I. Behnert, M. Schaale, J. Fischer, and, R. Doerffer, " Atmospheric correction algorithm for MERIS above case-2 waters, " Int. J. Remote Sens. **28**(7), 1469–1486 (2007).

8. J. Brajard, R. Santer, M. Crepon, and, S. Thiria, " Atmospheric correction of MERIS data for case 2 waters using neuro-variational inversion, " Remote Sens. Environ. **126**, 51–61 (2012).

9. M. Wang, S. Son, and, W. Shi, " Evaluation of MODIS SWIR and NIR-SWIR atmospheric correction algorithms using SeaBASS data, " Remote Sens. Environ. **113**, 635–644 (2009).

10. R. C. Smith and W. H. Wilson, "Ship and satellite bio-optical research in the Calofornia Bight," in *Oceanography from Space*, J. F. R. Gower, eds., (Plenum Publishing Corporation, New York), pp. 281–294 (1980).

11. R. W. Austin and T. Petzold, "The determination of the diffuse attenuation coefficient of sea water using the Coastal Zone Color Scanner," in *Oceanography from Space*, J. F. R. Gower, eds., (Plenum Publishing Corporation, New York), pp. 239–256 (1980).

12. B. Sturm, "The atmospheric correction of remotely sensed data and the quantitative determination of suspended matter in marine water surface layers," in *Remote Sensing in Meteorology, Oceanography and Hydrology*, A. P. Cracknel, eds., (Chister, UK: Ellis Horwood), pp. 163–197 (1981).

13. B. Sturm, "Selected topics of coastal zone color scanner (CZCS) data evaluation," in *Remote Sensing Applications in Marine Science and Technology*, A. P. Cracknel, eds., (Dordrecht, The Netherlands: D. Reidel), pp. 137–168 (1983).

14. M. Viollier and B. Sturm, "CZCS data analysis in turbid coastal water," J. Geophys. Res. **89**, 4977–4985 (1984).

15. A. Bricaud and A. Morel, "Atmospheric corrections and interpretation of marine radiances in CZCS imagery: Use of a reflectance model," Oceanol. Acta **33-50 N.SP**, (1987).

16. B. Sturm, V. Barale, D. Larkin, J. H. Andersen, and, M. Turner, "OCEAN code: the complete set of algorithms and models for the level 2 processing of European CZCS historical data, " Int. J. Remote Sens. **20**(7), 1219–1248 (1999).

17. J. M. Nicolas, P. Y. Deschamps, H. Loisel, and, C. Moulin, "POLDER-2: Ocean Color Atmospheric correction Algorithms, "Version 1.1. Algorithm Theoretical Basis Document, LOA, pp.17 (2005).

18. K. G. Ruddick, F. Ovidio, and, M. Rijkeboer, "Atmospheric correction of SeaWiFS imagery for turbid coastal and inland waters," Appl. Opt. **39**, 897–912 (2000).

19. K. G. Ruddick, V. De Cauwer, Y. Park, and, G. Moore, "Seaborne measurements of near infrared water-leaving reflectance: The similarity spectrum for turbid waters," Limnol. Oceanogr. **51**, 1167–1179 (2006).

20. M. Wang, W. Shi, and, L. Jiang, "Atmospheric correction using near-infrared bands for satellite ocean color data processing in the turbid western pacific region," Opt. Express **20**, 741–753 (2012).

21. Z. Lee, B. Lubac, J. Werdell, and, R. Arnone, "An update of the Quasi-Analytical Algorithm (QAA v5), " available at: `http://www.ioccg.org/groups/Software_OCA/QAA_v5.pdf` (2009).

22. C. Goyens, C. Jamet, and, K. Ruddick, "Spectral relationships for atmospheric correction. II. Improving NASA's standard and MUMM near infra-red modeling schemes, " accepted for publication in Opt. Express (2013).

23. M. Doron, S. Bélanger, D. Doxaran, and, M. Babin, "Spectral variations in the near-infrared ocean reflectance," Remote Sens. Environ. **115**, 1617–1631 (2011).

24. A. Morel and L. Prieur, "Analysis of variations in ocean color, " Limnol. Oceanogr. **22**, 709–722 (1977).

25. B. Sturm, G. Maracci, P. Schlittenhardt, C. Ferrari, and, L. Alberotanza, "Chlorophyll-a and total suspended matter concentration in the North Adriatic Sea determined from Nimbus-7 CZCS," paper presented at the Statutory Meeting, Int. Counc. for Explor. of the Sea, Woods Hole, Mass:, Oct. 6-12, (1981).

26. A. Morel and B. Gentili, "Diffuse reflectance of oceanic waters. III. Implication of bidirectionality for the remote-sensing problem, " Appl. Opt. **35**, 4850–4862 (1996).

27. C. D. Mobley, "Estimation of the remote-sensing reflectance from above-surface measurements," Appl. Opt. **38**, 7442–7455 (1999).

28. L. Kou, D. Labrie, and, P. Chylek, "Refractive indices of water and ice in the 0.65 mm to 2.5 mm spectral range," Appl. Opt. **32**, 3531–3540 (1993).

29. W. Shi and M. Wang, "An assessment of the black ocean pixel assumption for MODIS SWIR bands," Remote Sens. Environ. **113**, 1587–1597 (2009).

30. M. Wang, S. Son, and, L. W. Harding Jr., "Retrieval of diffuse attenuation coefficient in the Chesapeake Bay and turbid ocean regions for satellite ocean color applications," J. Geophys. Res. **114**, c10011 (2009).

31. M. Wang, J. Ahn, L. Jiang, W. Shi, S. Son, Y. Park, and, J. Ruy, "Ocean color products from the Korean Geostationary Ocean Color Imager (GOCI)," Opt. Express **21**(3), 3835–3849 (2013).

32. B. Nechad, K. Ruddick, and, Y. Park, "Calibration and validation of a generic multisensor algorithm for mapping

of total suspended matter in turbid waters," Remote Sens. Environ. **114**, 854–866 (2010).

33. H. Loisel, X. Mériaux, A. Poteau, L. F. Artigas, B. Lubac, A. Gardel, J. Caillaud, and, S. Lesourd, "Analyze of the inherent optical properties of French Guiana coastal waters for remote sensing applications," J. Coastal Res. **56**, 1532–1536 (2009).

34. V. Vantrepotte, H. Loisel, X. Mériaux, C. Jamet, D. Dessailly, G. Neukermans, D. Desailly, C. Jamet, E. Gensac, and, A. Gardel, "Seasonal and inter-annual (1998-2010) variability of the suspended particulate matter as retrieved from satellite ocean color sensors over the French Guiana coastal waters," J. Coastal Res. **64**, 1750–1754 (2011).

35. D. Doxaran, J. M. Froidefond, and, P. Castaing, "Remote-Sensing reflectance of turbid sediment-dominated waters," Appl. Opt. **42**(15), 2623–2634 (2003).

36. D. Doxaran, N. Cherukuru, and, S. J. Lavender, "Apparent and inherent optical properties of turbid estuarine waters: measurements, empirical quantification relationships and modeling," Appl. Opt. **45**(10), 2310–2324 (2006).

37. H. R. Gordon, O. B. Brown, R. H. Evans, J. W. Brown, R. C. Smith, K. S. Baker, and, D. K. Clark "A semianalytic radiance model of ocean color," J. Geophys. Res. **93**, 10909–10924 (1988).

38. A. Bricaud, A. Morel, M. Babin, K. Allali, and, H. Claustre, "Variations of light absorption by suspended particles with the chlorophyll a concentration in oceanic (case 1) waters: Analysis and implications for bio-optical models," J. Geophys. Res. **103**, 31033–31044 (1998).

39. K. L. Carder, F. R. Chen, Z. P. Lee, S. K. Hawes, and, D. Kamykowski, "Semianalytic Moderate-Resolution Imaging Spectrometer algorithms for chlorophyll a and absorption with bio-optical domains based on nitrate-depletion temperatures," J. Geophys. Res. **104**, 5403–5422 (1999).

40. Jr. R. W. Gould, R. A. Arone, and, P. M. Martinolich "Spectral dependence of the scattering coefficient in case 1 and case 2 waters," Appl. Opt. **38**(12), 2377–2383 (1999).

1. Introduction

The marine reflectance measured just above the water surface, $\rho_w(\lambda)$ (also referred to as $\rho_w^{0+}(\lambda)$ or normalized water-leaving reflectance [1]), retrieved from ocean color satellite images, allows to estimate biogeochemical parameters with a high revisit frequency and over large areas of oceans. The accuracy of these parameters depends however on the processing of the sensor-measured radiance, $L(\lambda)$, at the top of the atmosphere (TOA) used to obtain $\rho_w(\lambda)$. This processing includes, among others, the removal of the atmospheric contribution, the so-called atmospheric correction (AC) [1]. The top of atmosphere reflectance, $\rho^{TOA}(\lambda)$, is derived from the sensor-measured radiance and corrected for gas absorption, Rayleigh scattering, white-caps reflection and sun glint, to obtain the Rayleigh corrected reflectance, $\rho_{rc}^{TOA}(\lambda)$ [1]:

$$\rho_{rc}^{TOA}(\lambda) = \rho_a^{TOA}(\lambda) + \rho_{ra}^{TOA}(\lambda) + t_{\theta_v}(\lambda)t_{\theta_0}(\lambda)\rho_w(\lambda) \tag{1}$$

where $\rho_a^{TOA}(\lambda)$ and $\rho_{ra}^{TOA}(\lambda)$ represent the scattered sunlight by the aerosols and the coupling between both air and aerosol molecules, respectively. $t_{\theta_v}(\lambda)$ is the diffuse transmittance of the atmosphere along the viewing direction and $t_{\theta_0}(\lambda)$ is the diffuse transmittance of the atmosphere along incident direction. According to Eq. (1), if the optical properties and the concentrations of the aerosols are known, the quantities $\rho_a^{TOA}(\lambda)$, $\rho_{ra}^{TOA}(\lambda)$, $t_{\theta_0}(\lambda)$ and $t_{\theta_v}(\lambda)$ can be estimated and hence $\rho_w(\lambda)$ can be calculated.

At the time of the Coastal Zone Color Scanner (CZCS) satellite, the initial AC procedure assumed zero $\rho_w(\lambda)$ at 670 nm allowing to retrieve the atmospheric contributions from the total signal [2] (hereafter referred to as the black pixel assumption). With the addition of near infrared (NIR) bands for the next generation of ocean color satellite sensors (e.g., SeaWiFS, MODIS and MERIS), the 700-900 nm spectral range was used to estimate the aerosol contributions in the AC processes. Gordon and Wang [1] suggested to apply the black pixel assumption to the NIR spectral bands allowing to estimate $\rho_a^{TOA}(\lambda_{NIR})$ and $\rho_{ra}^{TOA}(\lambda_{NIR})$ and to select the appropriate aerosol optical models (hereafter referred to as the GW94 AC procedure). However in highly productive and turbid waters, due to absorption and backscattering of significant loads of algal and non-algal water constituents, the assumption of zero $\rho_w(\lambda)$ is not valid neither in the red nor in the NIR region of the spectrum [3, 4]. Assuming zero red or NIR $\rho_w(\lambda)$ in

such water masses leads to an overcorrection of the atmospheric effects and subsequently to an underestimation of $\rho_w(\lambda)$ [3].

To avoid the inappropriate application of the black pixel assumption, numerous red or NIR-modeling schemes have been developed to account for non-zero red or NIR $\rho_w(\lambda)$ within the AC processes. The standard NASA AC procedure for the processing of SeaWiFS and MODIS Aqua images, for instance, is a GW94-based AC procedure which includes a NIR-modeling iterative scheme with a bio-optical model to retrieve $\rho_w(\lambda_{NIR})$ where the black pixel assumption is not valid [4, 5]. Other AC approaches have also been suggested, e.g., coupled ocean-atmosphere optimization methods, such as the the direct inversion approaches using artificial neural networks [6–8]. For MODIS Aqua, the black pixel assumption was successfully applied in the Short-Wave-Infra-Red (SWIR) spectral domain where even turbid seawater appears to be totally absorbent [9].

Another approach to extent the GW94 AC procedure to turbid waters, consists of forcing the AC process with spectral relationships estimating red or NIR $\rho_w(\lambda)$ by means of $\rho_w(\lambda)$ at shorter wavelengths (i.e., $\rho_w(\lambda_j) = f(\rho_w(\lambda_i))$). These relationships reflect thus the spectral dependence of the marine signal itself, including the spectral dependence of the total absorption and backscattering simultaneously. Hence, it does not require retrieval of inherent optical properties. Moreover, it can be easily implemented in current red or NIR-modeling schemes to improve $\rho_w(\lambda)$ retrievals where current AC algorithms fail.

For the CZCS AC, empirical spectral relationships have been proposed to estimate $\rho_w(670)$ from $\rho_w(\lambda)$ in the blue and green region of the spectrum (hereafter referred to as red spectral relationships) [10–16]. An empirical spectral relationship was also used by Nicolas et al. [17] within the AC procedure of the POLarization and Directionality of the Earth's Reflectances-2 (POLDER-2) sensor. Similarly, several studies investigated the spectral dependence of the marine reflectance in the NIR region of the spectrum to model $\rho_w(\lambda_{NIR})$ for the AC of second generation ocean color satellite images (hereafter referred to as the NIR spectral relationships) [18–20]. Lee et al. [21] also suggested to correct remote sensing $\rho_w(667)$ estimations (due, for instance, to imperfect AC) for the Quasi-Analytical Algorithm by means of spectral relationships between $\rho_w(667)$ and $\rho_w(555)$.

Most of these spectral relationships have been developed with restricted datasets and have not been confirmed theoretically nor validated with independent *in situ* datasets. An overview and validation of these different red and NIR marine spectral relationships are thus essential to verify if these relationships are globally valid and if they can be used to improve AC for past, present and future ocean color sensors. In a companion paper, Goyens et al. [22] investigate how these spectral relationships can be implemented in current NIR-modeling schemes [5, 18, 19] to improve AC processes in turbid coastal waters.

In the present study, the AC literature is reviewed from the launch of the CZCS satellite till today giving a non-exhaustive list of various red and NIR spectral relationships used to estimate the water signal in the red (Section 2) and the NIR spectral region (Section 3) from $\rho_w(\lambda)$ at shorter wavelengths. Most spectral relationships encountered in the literature were initially developed for the CZCS sensor to retrieve $\rho_w(\lambda_{red})$. However, since the CZCS spectral bands are relatively close to the second generation satellite sensor spectral bands (e.g., SeaWiFS, MODIS Aqua or MERIS), these CZCS-oriented spectral relationships may eventually lead to red spectral relationships also valuable to constrain actual NIR-modeling schemes (e.g., the iterative scheme suggested by Stumpf et al. [4] and Bailey et al. [5] modeling $\rho_w(\lambda_{NIR})$ according to $\rho_w(\lambda_{red})$).

With the arrival of SWIR ocean color bands, a similar exercise could be performed to evaluate spectral relationships allowing to estimate $\rho_w(\lambda)$ in the NIR from $\rho_w(\lambda)$ in the SWIR spectral domain, and inversely. However, the present study is limited by the spectral range of

the *in situ* reflectance measurements, notably, from 400 to 900 nm, and is thus valuable for sensors with visible and NIR spectral bands (e.g., SeaWiFS, MODIS and MERIS sensors, the SEVIRI instrument on MSG, the Geostationary Ocean Color Imager (GOCI) and possibly the future GOCI-2 carried by COMS) as well as for studies covering decadal time scales including data from past and current sensors.

After reviewing the red and NIR spectral relationships, *in situ* reflectance spectra are described and their selection is outlined ensuring highly accurate reflectance spectra (Section 4). Next, red and NIR spectral relationships are validated (Section 5). A similar exercise has been done by Doron et al. [23] with *in situ*, remote sensing and simulated data. However the authors only focussed on the constant NIR reflectance ratio suggested by Ruddick et al. [18, 19]. Here a comprehensive overview and validation of 16 spectral relationships encountered in the literature are proposed.

2. Red spectral relationships

Initially the CZCS AC algorithm used the spectral band at 670 nm to estimate the aerosol contribution [2]. However, at 670 nm, both atmospheric and marine turbidity affect the TOA signal making it difficult to estimate either the aerosol content or the water reflectance with this single band [15]. Therefore, red-modeling schemes have been developed based on, e.g., spectral relationships to estimate the water signal at 670 nm from $\rho_w(\lambda)$ at shorter wavelengths. Smith and Wilson [10] and Austin and Petzold [11] related $\rho_w(670)$ with the reflectance ratio $\rho_w(443)/\rho_w(550)$ and the amplitude of reflectance at either 443 or 520 nm (Table 1). According to Austin and Petzold [11] using the reflectance at 520 nm was more appropriate to account for variations in non-algal particles while the ratio $\rho_w(443)/\rho_w(550)$ accounts for the pigment concentrations.

In the open ocean, the optical properties are essentially dominated by phytoplankton (often referred to as Case 1 waters) while in optically complex waters, the optical properties are dominated by other constituents such as dissolved organic matter and suspended sediments (often referred to as Case 2 waters) [24]. Hence, Sturm [13] proposed an iterative approach to solve the AC suggesting three equations according to the water type. The three equations are of the same type (Table 1). $\rho_w(670)$ is estimated from the water reflectance at 550 nm and an average blue-green ratio function β related to the total suspended matter (TSM) [14, 25]. The empirically defined constant terms of the equations were based on previous works and differed for clear waters [11], turbid near coastal waters [12] and *in situ* measurements taken in the northern Adriatic Sea (AAOT data) [12].

Viollier and Sturm [14] observed simple linear relations between $\rho_w(670)$ and $\rho_w(550)$ as a function of the water type. In the turbid coastal waters of the eastern English Channel, $\rho_w(670)$ represented 40% of $\rho_w(550)$ while, over a coccolithophorid bloom, it represented only 15%. In order to satisfy both water types, Viollier and Sturm [14] proposed a non-linear relationship similar to Smith and Wilson [10] and Austin and Petzold [11], but including the $\rho_w(520)/\rho_w(550)$ ratio instead of the blue-green ratio $\rho_w(443)/\rho_w(550)$ (Table 1).

Similarly to Sturm [13], Bricaud and Morel [15] demonstrated that AC could be improved by discriminating between Case 1 and Case 2 waters in the red-modeling scheme. They suggested several functions according to the water type, relating the Chlorophyll-a (Chl_a) absorption bands ratio $\rho_w(443)/\rho_w(670)$ and the blue-green ratio $\rho_w(443)/\rho_w(550)$ (Table 1). When the water type could not be defined as turbid or clear, Bricaud and Morel [15] used an intermediate relationship similar to the model of Smith and Wilson [10] (Table 1).

The OCEAN code, developed to process the level-2 European CZCS historical data [16], used both the relations of Viollier and Sturm [14] and Bricaud and Morel [15] within the red-modeling scheme to correct CZCS images for atmospheric contribution in turbid waters.

According to a first guess for $\rho_w(443)$ (based on the Black Pixel Assumption), the algorithm iterates with either the reflectance function of Viollier and Sturm [14] ($\rho_w(443) < 3.10^{-5}$) or the function of Bricaud and Morel [15] ($\rho_w(443) > 3.10^{-5}$) to account for non-zero $\rho_w(670)$.

Inspired by the CZCS red-modeling scheme proposed by Viollier and Sturm [14], Nicolas et al. [17] proposed an operational AC algorithm for POLDER-2 including a linear relationship between the marine signal at 565 and 670 nm (Table 1). The authors estimated $\rho_a(670)$ as the difference between the observed and modeled $\rho_w(\lambda)$. According to Nicolas et al. [17], this approach was satisfactory for most cases except for waters with high yellow substance absorption.

The Quasi Analytical Algorithm (QAA v.5) [21], used to derive the inherent optical properties from satellite $\rho_w(\lambda)$ estimations, includes three spectral relationships to correct erroneous satellite retrieved $\rho_w(667)$. $\rho_w(667)$ values are constrained within an upper and lower range defined by two spectral functions relating $\rho_w(\lambda)$ at 667 and 555 nm (Table 1). When the retrieved $\rho_w(667)$ is missing or out of limit, $\rho_w(667)$ is estimated from $\rho_w(555)$ and the ratio $\rho_w(490)/\rho_w(555)$ (Table 1).

As observed in Table 1, some spectral relationships are written in terms of sub-surface radiance, $L_{ss}(\lambda)$ or remote sensing reflectance, $R_{rs}(\lambda)$. For data analysis all functions are expressed here in terms of $\rho_w(\lambda)$. $L_{ss}(\lambda)$ and $R_{rs}(\lambda)$ are converted into $\rho_w(\lambda)$ following Morel and Gentili, [26] and considering the approximation for the ratio $(1 - r_F)/n_w$ (with r_F being the Fresnel reflectance and n_w the water refractive index) suggested by, e.g., Bricaud and Morel [15], Morel and Gentili [26], and Mobley [27].

3. NIR spectral relationships

Constant reflectance ratios in the NIR region of the spectrum were suggested by Ruddick et al. [18]. With assumptions on the backscattering and absorption in the NIR, the authors approximated $\rho_w(\lambda_1)/\rho_w(\lambda_2)$ by the water absorption ratio $a_w(\lambda_2)/a_w(\lambda_1)$ (with λ_1 and λ_2 being two wavelengths in the NIR). Ruddick et al. [19] further investigated these assumptions with radiative transfer simulations as well as above-water *in situ* measurements. The authors concluded that the NIR reflectance spectral shape is almost invariant for moderate turbidity and observed, as a function of λ_1 and λ_2, a constant reflectance ratio $\alpha(\lambda_1, \lambda_2)$ (Table 1). Accordingly, normalizing the reflectance spectra to the reflectance at a single wavelength in the NIR (referred by the authors to as the similarity NIR reflectance spectrum) allows to determine, at any wavelength, the water leaving reflectance shape in the NIR. This assumption is used to extent the GW94 AC process to turbid waters (hereafter referred to as the MUMM NIR-modeling scheme) [18, 19].

Ruddick et al. [19] also suggested theoretical values for $\alpha(\lambda_1, \lambda_2)$ based on the pure water absorption spectrum of Kou et al. [28] for the MUMM NIR-modeling scheme of MODIS, MERIS and SeaWiFS. However, the similarity NIR reflectance spectrum assumption appeared to be only valid for a certain range of turbidity. Indeed, variations in $\alpha(\lambda_1, \lambda_2)$ were observed when the NIR reflectance values were outside the 10^{-4} - 10^{-1} range [19]. A similar conclusion was made by Shi and Wang [29] who observed a quasi linear relationship between $\rho_w(645)$ and $\rho_w(859)$ for $\rho_w(859)$ values below 0.03. For waters with $\rho_w(859)$ above this threshold, $\rho_w(\lambda)$ at 645 nm saturated and remained almost constant (~ 0.012). Doron et al. [23] also observed some deviations from the constant reflectance ratio with both *in situ* and satellite derived data. According to that study, for $\rho_w(865)$ between 10^{-4} and 10^{-2}, $\alpha(765, 865)$ varied little between 1.73 and 1.84 as suggested by Ruddick et al. [19], but decreased with an increase in turbidity.

Wang et al. [20] proposed an NIR-modeling scheme for the AC of the Korean Ocean Satellite GOCI including a polynomial relationship between the water signal at 748 and 869 nm (Table 1, hereafter referred to as the GOCI NIR-modeling scheme). Initially, $\rho_w(\lambda)$ is retrieved with the GW94 AC algorithm allowing to calculate the water diffuse attenuation coefficient at 490

Table 1. Review of the spectral relationships and their applications

Source	Relation	Constant	Empirical/Theoretical	Application
Smith and Wilson (1980)	$L_{ss}(670) = aL_{ss}(443) \times \left[\frac{L_{ss}(443)}{L_{ss}(550)}\right]^b$	a=0.083 and b=-1.66	Empirical	CZCS AC
Austin and Petzold (1980)	$L_{ss}(670) = aL_{ss}(520) \times \left[\frac{L_{ss}(443)}{L_{ss}(550)}\right]^b$	a=0.0746, b=-0.919	Empirical	CZCS AC
Austin and Petzold (1980) in Sturm (1983)	$L_{ss}(670) = L_{ss}(550) \times 10^{-(a+b(\log(\beta))+c(\log(\beta))^2}$ with $\beta = d\frac{L_{ss}(443)}{L_{ss}(550)} + e\frac{L_{ss}(520)}{L_{ss}(550)} - f$	a=1.048, b=0.764, c=0.07 d=0.642, e=0.891, f=0.533	Empirical	CZCS AC clear water
Sturm (1981) in Sturm (1983)	$L_{ss}(670) = L_{ss}(550) \times 10^{-(a+b(\log(\beta))+c(\log(\beta))^2}$ β see Austin and Petzold (1980)	a=1.177, b=1.168, c= 0.292	Empirical (SPM >4-5 mg l^{-1})	CZCS AC turbid water
Sturm (1981) in Sturm (1983)	$L_{ss}(670) = L_{ss}(550) \times 10^{-(a+b(\log(\beta)))}$ β see Austin and Petzold (1980)	a=0.881, b=0.816	Empirical	in situ data in northern Adriatic Sea
Viollier and Sturm (1984)	$L_{ss}(670) = aL_{ss}(550)$	a=0.15	Empirical	$L_{ss}(\lambda)$ over Coccolithophorid bloom
	$L_{ss}(670) = aL_{ss}(550)$	a=0.40	Empirical	in situ data from coastal English Channel
Bricaud and Morel (1987)	$L_{ss}(670) = aL_{ss}(550) \times \left[\frac{L_{ss}(520)}{L_{ss}(550)}\right]^b$	a=0.23 and b=-2	Empirical	CZCS AC
	$\frac{L_{ss}(443)}{L_{ss}(670)} = a\left[\frac{L_{ss}(443)}{L_{ss}(550)}\right]^b$	a=5.89 and b=1.47	Empirical	Case 1 waters
	$\frac{L_{ss}(443)}{L_{ss}(670)} = a\left[\frac{L_{ss}(443)}{L_{ss}(550)}\right]^b$	a=14.55 and b=2.48	Empirical	Case 2 waters
	$\frac{L_{ss}(443)}{L_{ss}(670)} = a\left[\frac{L_{ss}(443)}{L_{ss}(550)}\right]^b$	a=6.73 and b=1.55	Empirical	Case 1 and 2 waters
Ruddick et al. (2000)	$\alpha = \frac{\rho_w(765)}{\rho_w(865)} = \frac{a_w(865)}{a_w(765)}$	α=1.72	Theoretical & empirical	SeaWiFS AC
Nicolas et al. (2005)	$\rho_w(670) = a\rho_w(565) + b$	a=0.20 and b=-0.0005	Empirical	Polder-2 AC
Ruddick et al. (2006)	$\alpha = \frac{\rho_w(\lambda_1)}{\rho_w(\lambda_2)}$	$\alpha = f(\lambda_1, \lambda_2)$	Theoretical & empirical	MODIS and SeaWiFS AC
Lee et al. (2009)	$R_{rs}(667) = aR_{rs}(555)^b$	Upper limit: a=20 and b=1.5 Lower limit: a=0.9 and b=1.7	Empirical	Upper and Lower bounds for $R_{rs}(667)$ in QAA v.5
Lee et al. (2009)	$R_{rs}(667) = aR_{rs}(555)^b + c\left[\frac{R_{rs}(490)}{R_{rs}(555)}\right]^d$	a=1.27, b=1.47, c=-0.00018 and d=-3.19	Empirical	QAA v.5 for missing/erroneous $R_{rs}(667)$
Wang et al. (2012)	$L_{wn}(869) = aL_{wn}(748) + bL_{wn}(748)^2$	a=0.368 and b=-0.040	Empirical	GOCI AC

nm, $K_d(490)$ [30]. Next, polynomial relations are used to estimate $\rho_w(748)$ from $K_d(490)$ and $\rho_w(869)$ from $\rho_w(748)$. These empirical relations were developed based on long term MODIS Aqua images over the turbid western Pacific region and processed with the NIR-SWIR GW94-based AC algorithm [9]. Although the GOCI NIR-modeling scheme provided satisfying results in the western Pacific region [20, 31], the polynomial relationship between $\rho_w(748)$ and $\rho_w(869)$ has not yet been validated with *in situ* data and applied to other coastal regions.

4. *In situ* data

Above-water reflectance measurements were made using TriOS-RAMSES hyperspectral radiometers during 63 sea campaigns undertaken between 2001 and 2012 (860 stations). Data were collected in coastal waters located in the southern North Sea and English Channel [32], the Celtic Sea, the Ligurian Sea, the Adriatic Sea and in the Atlantic Ocean along the coasts of Portugal and French Guyana [33, 34]. This dataset is particularly suitable for the validation of the spectral relationships as it includes measurements over contrasted and optically complex coastal waters. *In situ* data processing, averaging and selection are described in Ruddick et al. [19].

Out of the 860 stations, 105 *in situ* reflectance spectra satisfy the selection criteria and were not used by Ruddick et al. [19] for the calibration of the NIR similarity spectrum. Table 2 provides an overview of the minimum, maximum, average and standard deviation for $\rho_w(\lambda)$ of the selected spectra for the ocean color MODIS Aqua visible and NIR bands. The largest standard deviations in marine reflectance are encountered in the green and red region (Table 2). Around 869 nm the marine signal ranges from near zero to approximately 0.1, confirming the non-valid zero water-leaving reflectance assumption in the NIR. All spectra present $\rho_w(\lambda_{NIR})$ values above 10^{-4}, which is approximately the limit of validity for the black pixel assumption [3]. Out of the 105 spectra, 53% presents moderate turbidity with $\rho_w(869)$ ranging from 10^{-4} to 3.10^{-3} and 47% of the data presents very turbid waters with $\rho_w(869)$ exceeding 3.10^{-3}. This latter value corresponds to the threshold used by Wang et al. [9] to switch for the SWIR algorithm in the combined NIR-SWIR GW94-based AC algorithm.

Table 2. Statistics of the 105 $\rho_w(\lambda)$ (dimensionless) spectra for the ocean color bands of MODIS Aqua in the 412-869 nm range.

λ (nm)	min	max	mean	median	standard deviation
412	0.0069	0.0488	0.0230	0.0219	0.0114
443	0.0070	0.0642	0.0292	0.0301	0.0159
488	0.0080	0.0919	0.0414	0.0461	0.0234
531	0.0093	0.1144	0.0523	0.0594	0.0302
547	0.0084	0.1229	0.0568	0.0654	0.0334
667	0.0016	0.1309	0.0382	0.0316	0.0361
678	0.0018	0.1315	0.0376	0.0301	0.0359
748	0.0004	0.1134	0.0131	0.0061	0.0200
869	0.0002	0.0985	0.0079	0.0032	0.0148

Figure 1 shows the spectra in the 400-900 nm range and the red-NIR reflectance spectra normalized at 780 nm ($\rho_{wn780}(\lambda)$) as suggested by Ruddick et al. [18, 19]. Most spectra exhibit an increasing signal from the blue to the green region of the spectrum followed by a large peak between 550 and 600 nm [Fig. 1(a)]. A second peak is observed around 800 nm. Out of the 105 spectra, three spectra, taken in the Ligurian Sea, show a shape similar to clear ocean waters (peak in the blue followed by a decreasing signal with an increase in wavelength). In contrast, seven spectra present a lower peak around 550 and 600 nm and a higher peak around 690 nm followed by a relatively large signal at 800 nm and beyond.

According to Doxaran et al. [35], water masses with a reflectance spectrum showing a larger
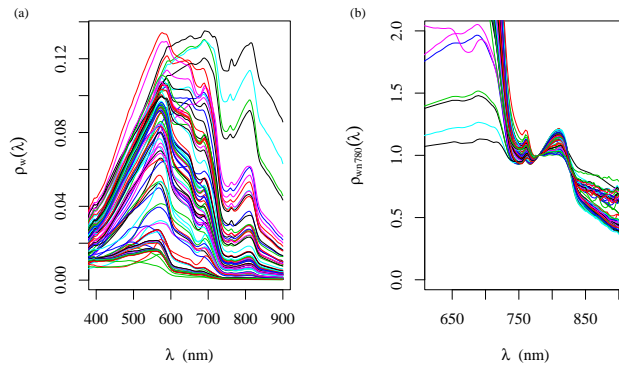
Fig. 1. Selected $\rho_w(\lambda)$ spectra between 400 and 900 nm and reflectance spectra normalized at 780 nm, $\rho_{wn780}(\lambda)$, in the 600-900 nm range.

peak at 550-600 nm are characterised by lower SPM values (< 100 mg l^{-1}), while water masses with a large reflectance peak around 700 and 800 nm present larger concentrations of SPM (> 100 mg l^{-1}). Indeed, these seven spectra are from the coastal waters of French Guiana known as being influenced by important river-discharge resulting in extremely turbid waters [33, 34]. These *in situ* measurements also exhibit distinctive $\rho_{wn780}(\lambda)$ spectra [Fig. 1(b)]. As observed by Ruddick et al. [19], most spectra present similar spectral shapes between 710 and 900 nm with a peak at 805-812 nm [Fig. 1 (b)]. The extremely turbid spectra from French Guiana instead show relatively lower $\rho_{wn780}(\lambda)$ values around 710 nm and often higher values at 850 nm and beyond.

5. Validation experiment

Spectral relationships are validated by comparing modeled and measured $\rho_w(\lambda)$ values qualitatively and quantitatively. The average percent relative error (RE), percent bias, root mean square error (RMSE), and R-squared coefficient (R^2) are calculated for each spectral relationship.

The percentage of data for which the RE does not exceed 10% of the observed value is also calculated as well as the validity ranges of each function in the visible. Validity ranges are determined by fitting a non-linear regression line through the observed and modeled $\rho_w(\lambda)$. The reflectance range for which the spectral relationship is satisfactory is defined by a difference between the regression and 1:1 line less than 10%.

5.1. Validation of spectral relationships in the visible

The statistical parameters comparing modeled and observed $\rho_w(670)$ are given in Table 3. Most functions tend to underestimate $\rho_w(670)$ (negative bias ranging from -3 to -63%). Two functions indicate a positive bias, notably, the function of Sturm [12] developed with AAOT data and the function of Viollier and Sturm developed with data from the English Channel (18 and 31%, respectively). However these spectral relationships overestimate $\rho_w(670)$ values below 0.05 but largely underestimate $\rho_w(670)$ values above this threshold. The relations from Smith and Wilson [10], Austin and Petzold [11], Bricaud and Morel [15] for the Case 2 waters, Nicolas et al. [17], and Viollier and Sturm [14] for the Coccolithophorid blooms show the lowest statistical performances. Statistics in Table 2 indicate that linear functions including a larger multiplication factor between the water signal in the red and the green spectral region result

in better $\rho_w(670)$ retrievals (Table 1). Indeed the relation of Viollier and Sturm [14] developed with *in situ* data from the English Channel (multiplication factor of 0.4) provides more satisfying results (see Table 2; lower bias, larger percentage of data with less than 10% RE and larger validity range) compared to the relations of Viollier and Sturm [14] over a coccolithophorid bloom (multiplication factor of 0.15) and Nicolas et al. [17] (multiplication factor of 0.2) (Table 1).

Table 3. Statistical performance of spectral relationships in the red (av. RE: average Relative Error, av. Bias: average Bias and RMSE: Root Mean Square Error)

	av. RE (%)	av. Bias (%)	RMSE	R^2 (%)	Percentage within 10%	Validity range
Smith and Wilson (1980)	60	-60	0.04	77	1	0-0.012
Austin and Petzold (1980)	63	-63	0.04	74	1	0-0.011
Austin and Petzold (1980) in Sturm et al. (1983)	34	-29	0.03	79	**27**	0-0.024
Sturm (1981) in Sturm et al. (1983), CZCS AC	**33**	-26	0.03	78	22	0-0.027
Sturm (1981) in Sturm et al. (1983), AAOT data	42	**18**	0.02	78	19	**0-0.043**
Viollier and Sturm (1984), Coccolithophorid bloom	51	-51	0.04	77	6	0-0.013
Viollier and Sturm (1984), English Channel	65	31	0.03	77	13	**0-0.036**
Viollier and Sturm (1984), CZCS AC	44	**-3**	0.03	**82**	8	**0-0.029**
Bricaud and Morel (1987), Case 1	41	-26	0.04	77	4	0-0.022
Bricaud and Morel (1987), Case 2	44	-44	0.04	74	7	0-0.019
Bricaud and Morel (1987), Case 1 and 2	39	-32	0.04	77	22	0-0.020
Nicolas *et al.* (2005)	48	-47	0.04	79	3	0-0.016
Lee *et al.* (2009) in QAA v.5	43	-43	0.04	**81**	4	0-0.020

As mentioned in Section 2, the algorithm described in the OCEAN code for the CZCS AC over turbid coastal waters [16] used the function of Viollier and Sturm [14] to model $\rho_w(670)$ when the retrieved $\rho_w(443)$ was below 3.10^{-5} and the Case 1 and 2 spectral relationships of Bricaud and Morel [15] otherwise. Although none of our *in situ* $\rho_w(443)$ values are below 3.10^{-5}, the reflectance function of Viollier and Sturm [14] yields better $\rho_w(670)$ retrievals (Table 3).

Similarly to the other spectral relationships, the relation suggested by Lee et al. [21] to estimate $\rho_w(667)$ when it is missing or erroneously retrieved (i.e, outside the bounding equations, Table 1), tends to underestimate larger $\rho_w(667)$ values. According to the R^2 this spectral relationship shows a relatively good fit with our *in situ* data (Table 3). However, the average bias and RE remain large (43% and -43%, respectively) and the percentage of values within 10% of the 1:1 line remains small (4%). In contrast, the bounding equations used by the authors to evaluate $\rho_w(667)$ according to $\rho_w(555)$ correspond to the limit of our *in situ* data [Fig. 2(a)].

Functions showing the best fit with the observed data are shown in Figs. 2(b)-2(d). These are the relations proposed by Austin and Petzold [11] and the two spectral relationships of Sturm [12] in [13]. The three relationships are of the same type (Table 1). They include the average blue green ratio β and the magnitude reflectance at 550 nm which can be related to the total absorption and the backscattering coefficient, respectively [14]. The maximum validity range in Table 3 and the plots in Figs. 2(b)-2(d) indicate that these functions largely underestimate $\rho_w(670)$ when the marine signal is greater than 0.03, which corresponds to very turbid waters ($\rho_w(869) \geq 3.10^{-3}$).

5.2. *Validation of NIR spectral relationships*

To evaluate the validity of the constant NIR reflectance ratios used in the MUMM NIR-modeling scheme [19], $\rho_w(\lambda_1)$ versus $\rho_w(\lambda_2)$ for the NIR bands of the SeaWiFS, MERIS and MODIS sensors are plotted in Figs. 3(a)-3(c). Ruddick et al. [19] suggested empirical and theoretical $\alpha(\lambda_1, \lambda_2)$ parameters derived from *in situ* measurements and from $a_w(\lambda)$ [28] (considering wavelength independent backscattering), respectively. With λ_1 taken in the red region of the
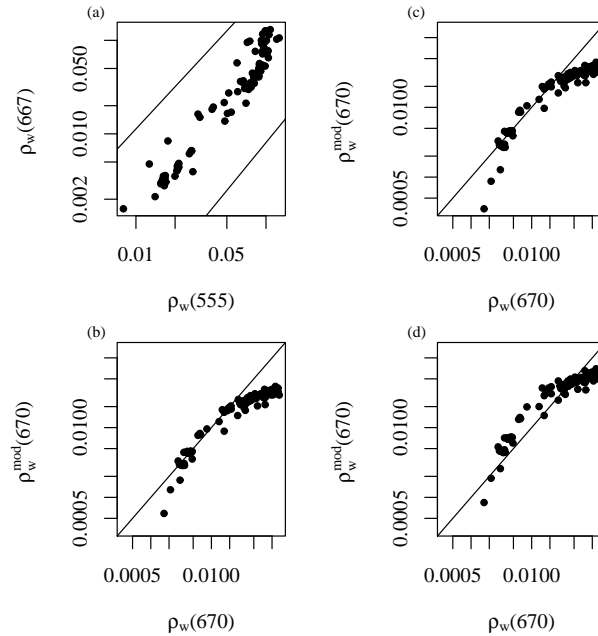
Fig. 2. (a) *In situ* $\rho_w(667)$ versus $\rho_w(555)$ including the upper and lower bounds to constrain $\rho_w(667)$ as suggested by Lee et al. (2009), and observed versus modeled $\rho_w(670)$ according to the spectral relationships suggested by (b) Austin and Petzold (1980) in Sturm (1983), (c) Sturm (1981, used for the CZCS AC over turbid waters) in Sturm (1983) and (d) Sturm (1981, developed with AAOT data) in Sturm (1983).

spectrum (600-700 nm range), constant reflectance ratios are valid for moderately/very turbid water with $\rho_w(\lambda_{NIR})$ below 10^{-2}. With λ_1 taken in the NIR region of the spectrum (700-800 nm range) the constant ratios are also valid for extremely turbid waters ($\rho_w(\lambda_{NIR}) > 10^{-2}$) [Figs. 3(a)-3(c)]. Accordingly, $\alpha(\lambda_1, \lambda_2)$ has a wider validity range when λ_1 is taken at longer wavelengths (> 750 nm). However, the constant $\alpha(\lambda_1, \lambda_2)$ values are not valid for $\rho_w(\lambda_{NIR})$ above 3.10^{-2}. $\rho_w(\lambda_{NIR})$ is systematically underestimated for these water masses [Figs. 3(a)-3(c)]. This suggests that one or more assumptions made by Ruddick et al. [18, 19] are not verified with the present dataset and result in variations of the reflectance ratio $\alpha(\lambda_1, \lambda_2)$ with turbidity. Indeed, Ruddick et al. [18, 19] assumed a negligible backscattering coefficient, $b_b(\lambda)$, compared to the absorption $a(\lambda)$ in the NIR region of the spectrum. However, in extremely turbid waters, $b_b(\lambda)$ may largely exceed $a(\lambda)$ resulting in an asymptote for $b_b(\lambda)/(b_b(\lambda)+a(\lambda))$ and subsequently in $\rho_w(\lambda)$. Since pure water absorption decreases with wavelength, the asymptote in $b_b(\lambda)/(b_b(\lambda)+a_w(\lambda))$ is reached earlier at shorter wavelengths, explaining the flattening of the ratios with turbidity as shown in Figs. 3(a)-3(c). This is in agreement with the observations of Doxaran et al. [36], who showed a flattening of the reflectance ratios $\rho_w(850)/\rho_w(550)$ and $\rho_w(850)/\rho_w(650)$ with increasing TSM concentrations, and with the conclusions of Shi and Wang [29], who observed a maxima in $\rho_w(675)$ for $\rho_w(859)$ values greater than 0.03.

Our results also confirm the observations of Doron et al. [23] who observed deviations from the constant ratios of $\rho_w(\lambda)$ in the NIR with variations in turbidity and mineral particle types.
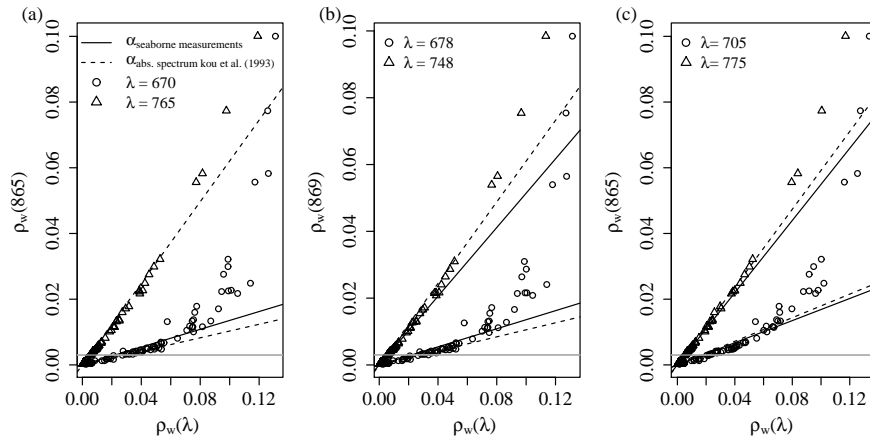
Fig. 3. Reflectance ratio in the red and the NIR for (a) SeaWiFS: $\rho_w(865)$ versus $\rho_w(670)$ and $\rho_w(765)$, (b) MODIS: $\rho_w(869)$ versus $\rho_w(678)$ and $\rho_w(748)$, and (c) MERIS: $\rho_w(865)$ versus $\rho_w(705)$ and $\rho_w(775)$. The constant $\alpha(\lambda_1, \lambda_2)$ suggested by Ruddick et al. (2006) based on *in situ* measurements and on $a_w(\lambda)$ (Kou et al., 1993) are represented for each reflectance ratio by a plain and dashed line, respectively. Horizontal grey lines indicate the limit between moderately turbid and very turbid waters (3.0^{-3})

.

Figures 4(a-b) show the NIR reflectance ratio for the SeaWiFS bands for moderately turbid and very turbid waters, respectively. Ruddick et al. [19] reported for this band ratio a constant $\alpha(765, 865)$ of 1.61 based on the pure water absorption model of Kou et al. [28]. Similarly to Doron et al. [23], we observe a larger NIR reflectance ratio in moderately turbid waters $(\alpha(765, 865) \sim 1.84)$ and a ratio closer to 1.61 for $\rho_w(865)$ values up to 10^{-2} [Fig. 4(b)]. For extremely turbid waters $(\rho_w(865) > 10^{-2})$, $\alpha(765, 865)$ is below 1.5 as noticed by Doron et al. [23].

Since the parameter $\alpha(\lambda_1, \lambda_2)$ appeared to vary with turbidity, the polynomial relationship suggested by Wang et al. [20], between $\rho_w(\lambda)$ at 748 and 869 nm (Table 1), may be more appropriate. Their function, developed with satellite data over the western Pacific region, is validated with our *in situ* data for moderately turbid and very turbid waters [Figs. 4(c) and 4(d)]. A RE of 10%, a small bias (-7%) and a R^2 of 99% are calculated between estimated and modeled $\rho_w(869)$. About 65% of the estimated $\rho_w(869)$ ranges within $\pm$ 10% of the corresponding observations. For moderately turbid waters, the constant NIR reflectance ratio of Ruddick et al. [19] and the polynomial function of Wang et al. [20] are close [Fig. 4(c)]. For very turbid waters, the function performs better than the constant NIR reflectance ratio [Fig. 4(d)]. However, the polynomial function could be further refined in order to enclose the most turbid data points where it underestimates $\rho_w(\lambda_{NIR})$ (see triangles in Fig. 4(d)).

6. Conclusion

The present study aimed to review spectral relationships in order to select appropriate functions which could be used as constraints to improve red or NIR-modeling schemes in current AC processes. Spectral relationships found in the literature were developed with restricted or regional datasets explaining the need of an accurate validation.

Sixteen published spectral relationships, estimating $\rho_w(\lambda)$ in the visible or NIR spectral region, were validated using 105 highly accurate *in situ* above-water reflectance measurements
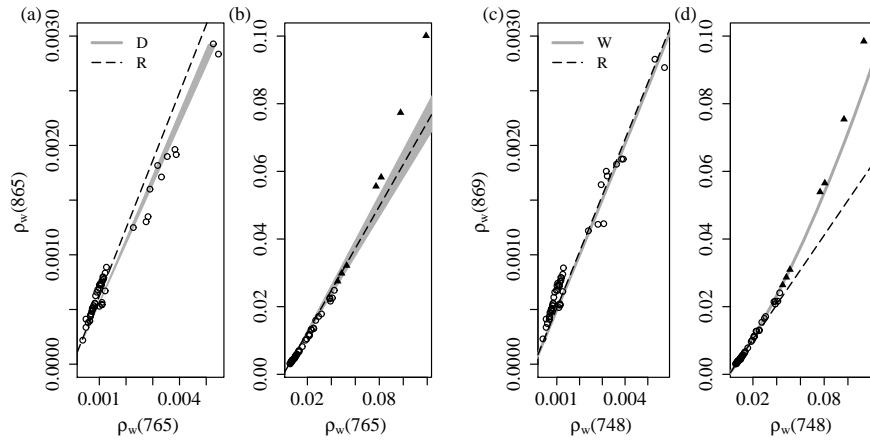
Fig. 4. $\rho_w(765)$ versus $\rho_w(865)$ according to Ruddick et al. (2006) (R, dashed line) and Doron et al. (2011) (D, grey bands) for (a) moderately turbid and (b) very turbid waters and $\rho_w(748)$ versus $\rho_w(869)$ for (c) moderately turbid and (d) very turbid waters with the polynomial function proposed by Wang et al. (2012) (W, plain grey line) and the constant ratio proposed by Ruddick et al. (2006) (R, dashed line). Spectra from extremely turbid coastal waters of French Guiana described in Section 4 are indicated by a triangle.

taken in diverse coastal water types. Functions used to model $\rho_w(\lambda)$ at 670 nm for CZCS AC processes [10–12, 15], systematically underestimated the water signal for very turbid waters. Similarly, the function suggested by Lee et al. [21] to estimate $\rho_w(667)$ from the water signal in the green and the blue-green reflectance ratio, tends to underestimate higher $\rho_w(667)$ values. In contrast, the bounding equations used in the latest version of the QAA, to evaluate maximum and minimum $\rho_w(667)$ estimations according to the water signal in the green, appear to be valid for the entire range of turbidity encountered in the *in situ* dataset.

In the NIR spectral region, the constant reflectance ratio $\alpha(\lambda_1, \lambda_2)$, suggested by Ruddick et al. [18, 19] to extend the GW94 AC algorithm to turbid waters, was valid for moderately to very turbid waters with $\rho_w(865 - 869)$ values below 10^{-2}, while the polynomial function of Wang et al. [20] was also valid for extremely turbid water masses. However, the latter slightly underestimated $\rho_w(869)$ for water masses with $\rho_w(\lambda_{NIR})$ exceeding 0.05.

From this study we can conclude that the red spectral relationships are not appropriate for the entire range of coastal turbidity encountered in our *in situ* dataset suggesting that either the red spectral functions need to be updated or that the functions should differ according to the optical water type and/or the turbidity range. In contrast, bounding equations, as suggested by Lee et al. [21], allow some variability and may thus be more appropriate to force red or NIR-modeling schemes within AC processes when a priori informations on the water type or turbidity levels are not available or when the AC procedure is expected to perform globally. The polynomial NIR function, initially developed with remote sensing reflectances over the Western Pacific [20], presented a satisfying fit with our *in situ* data.

The actual standard NASA CZCS AC procedure assumes a fixed aerosol type and includes an iteration scheme to estimate $\rho_w(670)$ from inherent optical properties at 555 nm and Chl_a concentration estimations [4, 37–40]. Hence, in turbid waters where $\rho_w(670)$ is not solely determined by algal particles, CZCS $\rho_w(\lambda)$ retrievals may be improved by forcing the iteration

scheme with the red bounding equations suggested by Lee et al. [21]. However, to further improve red-modeling schemes, more work into developing globally valid red spectral relationships is required.

For the second generation ocean color satellite images, bounding red and NIR polynomial spectral relationships may be used to improve NIR-modeling schemes in current AC algorithms (e.g., the iteration scheme in the standard NASA AC algorithm for MODIS Aqua [5] and the MUMM NIR-modeling scheme [18, 19]). How these spectral relationships may lead to improved $\rho_w(\lambda)$ retrievals, is investigated in the companion paper of this study by Goyens et al. [22].

Acknowledgments